


Anomalous electron transport in epitaxial NdNiO₃ films

Shashank Kumar Ojha, Sujay Ray, Tanmoy Das, and S. Middey*
Department of Physics, Indian Institute of Science, Bengaluru 560012, India

Sagar Sarkar and Priya Mahadevan
S.N. Bose National Center for Basic Sciences, JD-Block, Sector III, Salt Lake, Kolkata 700098, India

Zhen Wang and Yimei Zhu
Department of Condensed Matter Physics and Materials Science, Brookhaven National Laboratory, Upton, New York 11973, USA

Xiaoran Liu, M. Kareev, and J. Chakhalian
Department of Physics and Astronomy, Rutgers University, Piscataway, New Jersey 08854, USA

 (Received 8 April 2019; revised manuscript received 10 June 2019; published 27 June 2019)

The origin of simultaneous electronic, structural, and magnetic transitions in bulk rare-earth nickelates ($RENiO_3$) remains puzzling with multiple conflicting reports on the nature of these entangled phase transitions. Heterostructure engineering of these materials offers unique opportunity to decouple the metal-insulator transition (MIT) from the magnetic transition. However, the evolution of underlying electronic properties across these decoupled transitions remains largely unexplored. In order to address this, we have measured Hall effect on a series of epitaxial $NdNiO_3$ films, spanning a variety of electronic and magnetic phases. We find that the MIT results in only a partially gapped Fermi surface, whereas the full insulating phase forms below the magnetic transition. In addition, we also find a systematic reduction of the Hall coefficient R_H in the metallic phase of these films with epitaxial strain and also a surprising transition to a negative value at large compressive strain. The partially gapped, weakly insulating, paramagnetic phase is reminiscent of pseudogap behavior of high- T_c cuprates. The precursor metallic phase, which undergoes transition to the insulating phase, is a non-Fermi liquid with a temperature exponent n of resistivity of 1, whereas the exponent increases to $4/3$ in the noninsulating samples. Such a nickelate phase diagram with sign reversal of R_H , a pseudogap phase, and non-Fermi-liquid behavior is intriguingly similar to high- T_c cuprates, giving important guidelines to engineer unconventional superconductivity in oxide heterostructures.

DOI: [10.1103/PhysRevB.99.235153](https://doi.org/10.1103/PhysRevB.99.235153)

I. INTRODUCTION

The question about the nature of the metal-insulator transition (MIT) and spin ordering in the negative-charge-transfer family of materials $RENiO_3$ ($RE = Pr, Nd, \dots, Lu$, etc.) has drawn significant interest in the pursuit of understanding the ultimate connection among the underlying crystal structure and electronic and magnetic orderings [1–23]. Independently, there have been a number of interesting theoretical proposals to realize high-temperature superconductivity through epitaxial engineering [24–27], leading to remarkable progress in the synthesis and characterization of ultrathin films and heterostructures of rare-earth nickelates (for recent progress see Refs. [3,4] and references therein). Since the degeneracy lifting between two e_g orbitals of Ni^{3+} ions might lead to a cupratelike one-band Fermi surface, orbital engineering of $RENiO_3$ has also been attempted in various heterostructure forms [3,28–33]. However, to date, the maximum achieved orbital polarization of nickelate heterostructures ($\sim 25\%$) is still significantly smaller than what is required to engineer the material analog of high- T_c cuprates. Therefore, it is of

paramount interest to find out if and how epitaxy can be utilized to finally achieve cupratelike electronic structure in $RENiO_3$ -based heterostructures.

Hall effect is an important measurement which provides crucial information about the Fermi surface topology, the carrier concentration, the anisotropy of the scattering rate, and the chiral spin textures of quantum materials [34–37]. In connection to nickelates, earlier studies on bulk $NdNiO_3$ (NNO) and $PrNiO_3$ (PNO) powder samples demonstrated the phenomenon of sign change of the Hall coefficient R_H across the metal-insulator transition [38]. Interestingly, such evolution of R_H has also been observed in several important “bad” metals, including cuprates, vanadates, and ruthenates; this phenomenon was attributed to multiple factors, including structural transition, spin density wave (SDW) transition, and charge density wave transition [39–42]. Therefore, the simultaneous occurrence of MIT, structural transition, and charge and magnetic ordering in bulk NNO and PNO [6,43–45] inhibits the straightforward determination of the primary factor responsible for such a drastic change in R_H . On the other hand, these simultaneous transitions can be selectively decoupled or even suppressed by epitaxial strain in ultrathin-film geometry [12,13,15,46–48]. Naturally, in such

*smiddey@iisc.ac.in

a situation one can expect that Hall effect measurement will provide crucial information about the electronic and magnetic transitions. Further, it is interesting to note that epitaxial strain dramatically affects the electronic properties in the metallic phase of nickelate films, as highlighted by the change in the characteristic power exponents of resistivity, associated with the non-Fermi-liquid behavior [46,47,49]. This observation suggests that Hall effect measurements in the metallic phase can probe the relative change in Fermi-surface topology brought about by epitaxial strain [50].

In this paper, we report on the detailed Hall effect measurements across several electronic and magnetic phases of NNO, which have been realized in a series of epitaxially stabilized high-quality ultrathin films on several single-crystalline substrates. These measurements have revealed a direct link between the sign change of R_H and the onset of the E' antiferromagnetic (E' -AFM [45]) transition, implying a SDW origin of the puzzling E' -AFM phase. Such a magnetic transition driven by the Fermi surface reconstruction was predicted by earlier theoretical works [7,8]. Moreover, the metallic phase of the NNO film under large tensile strain exhibits unexpected cupratelike linearly T dependent resistivity and T^2 dependence of the cotangent of the Hall angle. The magnitude of R_H in the metallic phase shows a systematic decrease with the underlying strain and remains positive down to the lowest temperatures under moderate compressive strain. Upon application of a large compressive strain, surprisingly negative R_H for ($T > 60$ K) emerges in the metallic phase, emphasizing a drastic change in the Fermi surface topology. The decrease (increase) in hole (electron) concentration without any chemical doping illustrates a strain-mediated self-doping scenario, which is further verified by density functional theory (DFT). Our further analysis using the DFT plus momentum-resolved density fluctuation (MRDF) method found that the suppression of E' -AFM ordering by epitaxial strain can be accounted by the suppression of Fermi surface nesting.

II. METHODS

Ultrathin films of NNO [15 unit cells (u.c.)] of high structural and chemical quality were grown on several single-crystalline substrates [see Fig. 1(a)]: SrTiO₃ (STO), NdGaO₃ (NGO), SrPrGaO₄ (SPGO), SrLaAlO₄ (SLAO), and YAlO₃ (YAO). The details of the growth procedure can be found in Ref. [46]. The in-plane pseudocubic lattice constants of all the substrates used and the corresponding strain ϵ values are summarized in Fig. 1(b). The layer-by-layer growth was monitored by *in situ* reflection high-energy electron diffraction (see the Supplemental Material [51]), and the desired epitaxial growth along a pseudocubic [001] direction was confirmed by x-ray diffraction [51]. A sample for cross-section scanning transmission electron microscopy (STEM) measurement was prepared by a focused ion beam with Ga⁺ ions followed by Ar⁺ ion nanomilling. High-angle annular dark-field (HAADF) imaging was achieved with a JEOL ARM200 microscope equipped with two aberration correctors. Figure 1(c) shows a characteristic HAADF-STEM image taken across the NNO/NGO interface along the [100] direction. The atomic column intensity in the HAADF-STEM imaging varies with the atomic number as $\propto Z^{1.7}$; that is, heavier atoms indicate

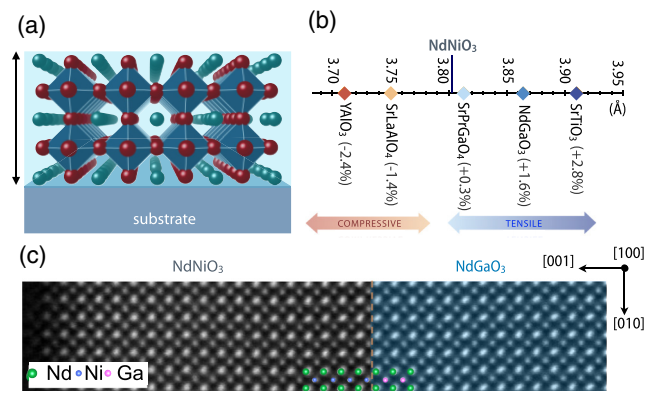


FIG. 1. (a) NdNiO₃ thin film on a single-crystalline substrate. (b) Pseudocubic in-plane lattice constant for the substrates used in this work and the corresponding epitaxial strain for NNO. (c) HAADF-STEM image (with false color) of a 20-u.c. NdNiO₃ film on a NdGaO₃ substrate.

brighter columns. As marked by the dashed line, the NGO substrate terminates with a NdO layer with a practically atomically sharp interface, which further testifies to the excellent registry between the sample and substrate. The dc resistivity and Hall effect measurements were carried out in four-probe van der Pauw geometry using a Quantum Design physical property measurement system. To evaluate R_H , magnetic field (H) was swept between ± 5 T at different T . In the absence of an anomalous Hall contribution, while the intrinsic Hall resistance R_{xy} should be zero at $H = 0$ and asymmetric with the magnetic field sweep, the finite width of the contacts adds an additional symmetric part in R_{xy} around $H = 0$ with a vertical offset [52,53]. These parasitic contributions were corrected to extract intrinsic R_{xy} , and three typical sets of such corrected R_{xy} curves as a function of H for different T are presented in the Supplemental Material [51]. As clearly seen, after correction, R_{xy} remains linear within the ranges of magnetic field H used in this work; the Hall coefficient is evaluated as $R_H = t(dR_{xy}/dH)$, where t is the film thickness.

To gain further insight into the change in R_H in the metallic phase of the samples as a function of epitaxial strain, we performed DFT calculation using the Vienna Ab initio Simulation Package (VASP) [54,55] within the generalized gradient approximation + U of the Perdew-Burke-Ernzerhof parametrization [56]. Projected augmented-wave [57,58] pseudopotentials were used to describe core electrons. We use $U = 3.5$ eV, which is larger than the values of U used in the self-energy calculation. This is expected since the bare U used in the self-energy calculation is further multiplied by various components of the susceptibility to provide the effective many-body potential in this calculation. The electronic wave function is expanded using plane waves up to a cutoff energy of 500 eV. Brillouin zone (BZ) sampling is done by using a $(12 \times 12 \times 6)$ Monkhorst-Pack k grid. Like in Ref. [46], NdNiO₃ crystal structures have been constrained to the $P4/mmm$ space group in our calculation, and A-type antiferromagnetic spin ordering on the Ni sublattice has been imposed, instead of the complex E' -AFM spin configuration. Octahedral tilts/rotations and breathing mode distortions have also been omitted in our calculations, and the effect of

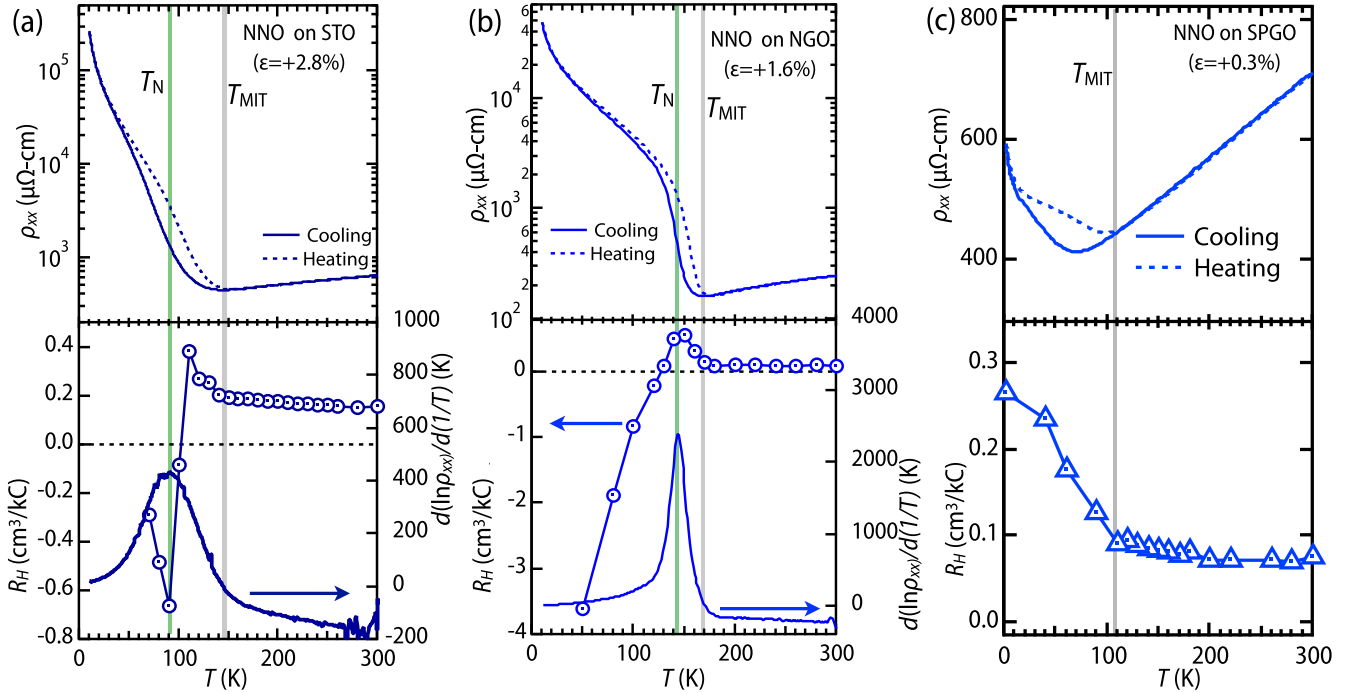


FIG. 2. (a)–(c) Temperature dependence of the dc resistivity of a 15-u.c. NNO film under tensile strain (top panel) and the variation of R_H (bottom panel). The right axis of the bottom panel of (a) and (b) corresponds to a $d(\ln\rho_{xx})/d(1/T)$ vs T plot.

substrates has been folded into the experimental lattice constants. Despite these constraints, such a DFT approach was shown to successfully reproduce the experimentally observed band structure and Fermi surface topology of NNO thin films on different substrates [59]. The effects of electronic correlations on the band structure have been investigated by DFT and DFT + self-energy corrections, obtained with MRDF theory (details of this calculation are given in the Supplemental Material) [59–62].

III. RESULTS AND DISCUSSION

A. Hall coefficient across electronic and magnetic transitions

The top panels of Figs. 2(a)–2(c) show the temperature-dependent resistivity of NNO films under tensile strain. As reported earlier [46,47], NNO films under tensile strain show the first-order MIT. The metal-insulator transition temperature T_{MIT} (defined as the temperature where $d\rho_{xx}/dT = 0$) and magnetic transition temperature T_N [evaluated from the $d(\ln\rho_{xx})/d(1/T)$ vs T plot on the right axis of the bottom panel of Figs. 2(a) and 2(b)] [63] of these films are listed in Table I. Note that the lower value of T_{MIT} compared to the

bulk NNO $T_{MIT} = T_N \sim 200$ K was linked to the effect of epitaxial strain (bandwidth control) and reduced dimensionality (quantum confinement) [46]. Moreover, previous reports using resonant x-ray scattering (RXS) on such NNO films confirmed the absence of both bulk-like charge ordering and lattice symmetry change across the MIT [13,15]. Separation between T_{MIT} and T_N of these samples offers a unique temperature window to examine the evolution of R_H across all three phases: paramagnetic metal, paramagnetic insulator, and antiferromagnetic insulator (AFI) without the influence of charge disproportionation and structural transition. While a bulk-like MIT and magnetic transition are expected in an epitaxial NNO film under a very small tensile strain of +0.3%, surprisingly, the film shows only weakly insulating, paramagnetic behavior at low temperature [46] [see top panel in Fig. 2(c)].

In the following, we discuss the overall response of R_H across the electronic and magnetic transitions of these films. The temperature dependence of ρ_{xx} and R_H in the metallic phase will be presented later in the text. As immediately seen in Figs. 2(a)–2(c), at room temperature R_H is holelike. Although the electronic structure of the system is expected to be drastically different across the metal-insulator transition, R_H exhibits only a slight increase across T_{MIT} for the NNO film on NGO and STO. Most interestingly, R_H switches to n -type around 100 K and 120 K for the STO and NGO cases, respectively, which are remarkably close to the respective T_N for E' -AFM ordering. A similar sign change of R_H across T_N was also observed in the $2\text{EuNiO}_3/1\text{LaNiO}_3$ superlattice, which has monoclinic symmetry in both metallic and insulating phases and does not exhibit any charge ordering transition [21]. R_H maintains holelike behavior even in the weakly insulating state for the film grown on the SPGO

TABLE I. Metal-insulator transition temperature T_{MIT} and antiferromagnetic ordering temperature T_N , evaluated from ρ_{xx} vs T data. c and h correspond to cooling and heating cycles, respectively.

Film	T_{MIT}^c (K)	T_{MIT}^h (K)	T_N^c (K)	T_N^h (K)
NdNiO ₃ on SrTiO ₃	145	155	90 ± 5	110 ± 5
NdNiO ₃ on NdGaO ₃	170	175	140	155

substrate, where earlier RXS experiments [46] clearly ruled out the appearance of E' -type magnetic ordering. All of these observations clearly point to some large changes in the Fermi surface topology being responsible for the appearance of E' -type antiferromagnetic ordering in these materials.

The mechanisms of the MIT and E' -type AFM ordering of $RENiO_3$ are still heavily debated [5–18,20–23]. Most recently, the MIT mechanism was attributed to the $d^8\bar{L} + d^8\bar{L} \rightarrow d^8 + d^8\bar{L}^2$ bond disproportionation (BD) transition (here \bar{L} denotes a ligand hole in O p bands) [5,10,11,14,17,21,64]. Apart from the BD-induced transition scenario, the importance of Mott physics in the realization of the insulating phase was found in optical conductivity measurements [9,64]. Another unexpected result was revealed in the recent valence band photoemission measurement, which showed the presence of residual intensity at E_F even at very low T , thus signaling that some parts of the Fermi surface still survive deep in the insulating phase [65]. Such a notion of a partially gapped Fermi surface, akin to the pseudogap phase of high- T_c cuprates, ruthenates, pnictides, etc. [66–68], was also inferred for NNO from infrared spectroscopy [9] and tunneling spectroscopy measurement [69].

Since R_H is magnetic field independent within the range of magnetic field used in the present study, it can be expressed as $R_H = (n_p\mu_p^2 - n_e\mu_e^2)/e(n_p\mu_p + n_e\mu_e)^2$, assuming one electron band and one hole band contribute to the electrical transport, where n_p (n_e) is the hole (electron) density and μ_p (μ_e) is the mobility of the hole (electron) [70]. The positive sign of R_H in the paramagnetic metallic phases [48,53,71] originates from the larger volume of the hole pockets (v_p) compared to that of the electron pockets (v_e) as observed in angle-resolved photoemission spectroscopy (ARPES) experiments [59,72]. A small increase of R_H upon entering the insulating phase suggests that the BD transition opens only a partial gap in the Fermi surface. ARPES measurement [72] found a strong instability at $\mathbf{q} = (1/4, 1/4, 1/4)_{p.c.}$, which also coincides with the magnetic wave vector for E' ordering. Thus, the nesting of dominant hole pockets in the BD phase opens a gap in the hole Fermi surface and results in the emergence of the E' -AFM phase [7,8,12,48,53,73], with the remaining electron pockets contributing to the transport to result in the observed switching of R_H across T_N . Once the BD phase and E' -AFM ordering set in, they act synergetically to grow together with the decrease of thermal fluctuations [74]. Complementary experiments, like ARPES measurements at different T , are required to fully understand the evolution of R_H with T in the AFI phase. On lowering tensile strain, the suppression of the Fermi surface superstructure at $(1/4, 1/4, 1/4)_{p.c.}$ is found to be responsible for the absence of the E' -AFM phase in the NNO film on a SPGO substrate, where R_H remains positive in such a paramagnetic BD phase (results are shown in the Supplemental Material [51]).

B. ρ_{xx} and R_H in the metallic phase

Next, we explore magnetotransport behavior in the metallic phase. Contrary to the expected T^2 dependence of resistivity at low temperature for a Fermi liquid, ρ_{xx} in the metallic phases of NNO under tensile strain shows *linear* T -dependent behavior (see the Supplemental Material [51]). As reported

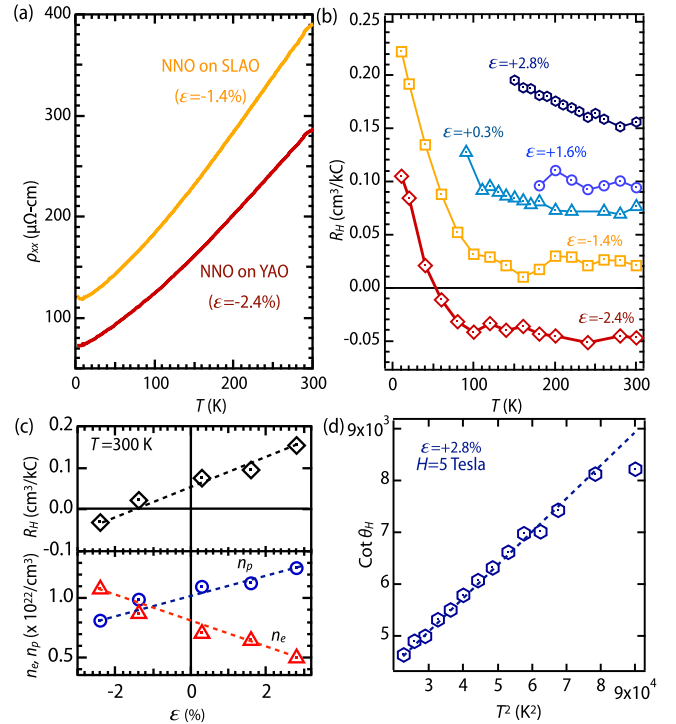


FIG. 3. (a) Temperature dependence of the dc resistivity for 15-u.c. NNO films under compressive strain. (b) Temperature dependence of R_H in the paramagnetic metallic phase of the NNO films. (c) Relation of R_H (top panel) and carrier density (bottom panel) with strain at 300 K. (d) $\cot \theta_H$ for the NNO film on a STO substrate as a function of T^2 . The dotted line represents the T^2 dependence.

earlier [46], the electronic and magnetic transitions can be entirely suppressed by the application of compressive strain [see Fig. 3(a)]. Interestingly, under compressive strain ρ_{xx} shows $T^{4/3}$ dependence over a broad range of temperatures and then switches to linear T behavior [51]. Such non-Fermi-liquid behavior has been observed in the normal phase of several unconventional superconductors, including cuprates, organic superconductors, pnictides, heavy fermions, etc. [75–78], and its intrinsic origin is still unknown [79,80].

The overall behavior of R_H in the metallic phase is summarized in Fig. 3(b). As can be seen, the NNO film grown on the SLAO substrate (-1.2%) exhibits a p -type metallic behavior over the entire temperature range. With the further increase of compressive strain (NNO on YAO), R_H surprisingly becomes negative even at 300 K. A systematic relation between $R_H|_{T=300\text{K}}$ and ϵ can be further inferred from the top panel of Fig. 3(c). Such strain-mediated change in carrier density shown in Fig. 3(c) is a hallmark of the self-doping effect [51].

For a normal metal, R_H generally becomes temperature independent for $T > 0.2\text{--}0.4 \Theta_D$ (Θ_D is the Debye temperature) [81]. Since, for $RENiO_3$, $\Theta_D \sim 420\text{ K}$ [82], a strong T -dependent R_H in the metallic phase of the NNO film on STO requires some special consideration. For this purpose we recall that in hole-doped cuprates the strong T dependence of R_H is commonly discussed in terms of the Hall angle $\cot \theta_H = \rho_{xx}/(HR_H)$. The T^2 dependence of the $\cot \theta_H$, observed

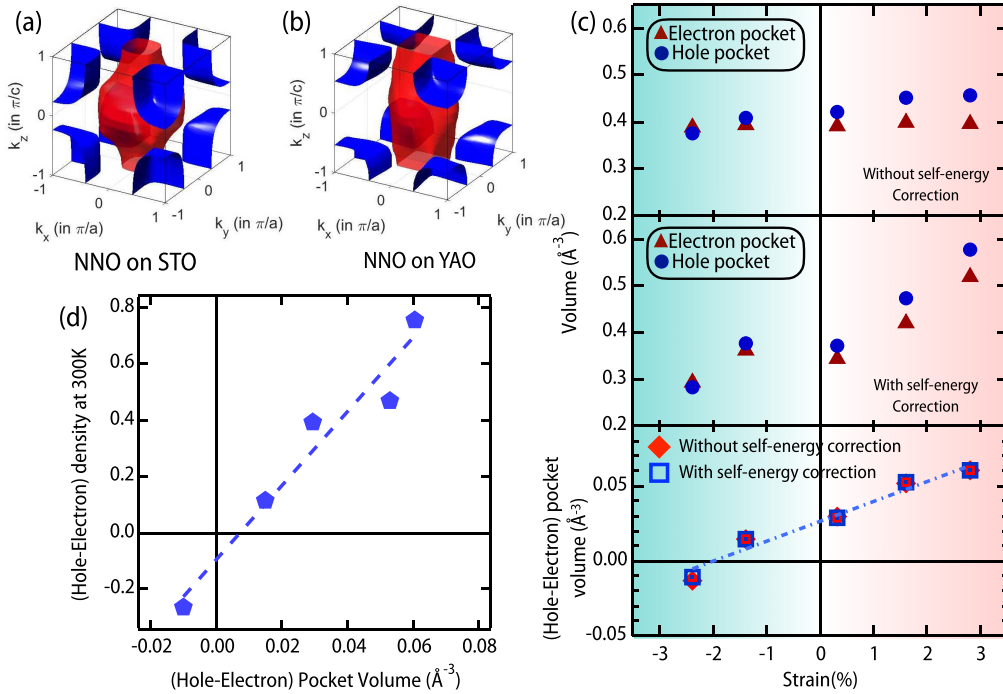


FIG. 4. (a) and (b) Computed FS topology for the two representative samples of NNO/STO and NNO/YAO. a in the x and y axes of these graphs corresponds to the in-plane pseudocubic lattice constant of the substrate. For the z axis, $c \sim 2c_{p.c.}$, where $c_{p.c.}$ is the out-of-plane lattice constant of the NNO film. Details of the Brillouin zone are discussed in the Supplemental Material [51]. (c) FS volumes for electron (triangle) and hole (circles) pockets compared for all samples without (top panel) and with (middle panel) self-energy corrections. The bottom panel compares the difference between the hole and electron pocket volumes for calculations without (solid diamonds) and with (open squares) self-energy effects. (d) Comparison of the difference between the two FS volumes with the experimental value of the effective carrier density obtained from the Hall effect.

in hole-doped cuprates around optimal doping, has been interpreted as a signature of spin-charge separation or the result of anisotropic scattering rates [81,83–86]. However, R_H becomes T independent in lightly hole doped cuprates, and consequently, $\cot \theta_H$ follows the T dependence of ρ_{ab} [35]. Based on these results, we can speculate that the T^2 dependence of $\cot \theta_H$ [Fig. 3(c)] and the linear T dependence of ρ_{xx} for the NNO film on STO implies a strong connection to the “strange-metal” phase of high- T_c cuprates. As shown in Fig. 3(b), with the decrease of hole concentration, R_H becomes almost T independent in the metallic phase of the NNO film on NGO and at high temperatures for other compressive substrates. The sharp increase in R_H below 100 K in compressively strained NNO can be attributed to the emergence of the pseudogap phase [69,87], which is observed in many cuprates and yet is a poorly understood phenomenon [35,84,88–90]. In addition, the sign change of R_H in the pseudogap phase suggests that there is a coexistence of electron and hole Fermi surface pockets with different mobilities, as also seen in electron- and hole-doped cuprates [39,91–93]. Our result further implies that the hole pocket has higher mobility compared to the electron pocket, which is consistent with prior ARPES data [72].

C. DFT calculation

In order to gain insight into the strain-induced modulation of R_H in the metallic phase shown in Fig. 3(c), we have

calculated the Fermi surface (FS) of NNO for different values of ϵ , listed in Fig. 1(b). In all cases, we obtain a characteristic FS topology which consists of the electron pocket at the center of the BZ and hole pockets at the zone corners. The computed FSs shown in Figs. 4(a) and 4(b) for large tensile (STO) and large compressive (YAO) strain exhibit the characteristic reduction of the three-dimensionality of the electron pocket (the electron pocket is almost cylindrical for NNO on YAO) as a function of strain. In Figure 4(c), we summarize the evolution of FS volumes for the two pockets. As seen, despite the gradual loss of three-dimensionality in Fermi surface between NNO under +2.8% and NNO under –2.4%, the electron pocket volume remains essentially unchanged. On the other hand, the hole pocket volume is larger than the electron pocket volume for all cases except for NNO on YAO. This is the key mechanism for the sign change in the Hall coefficient at high temperatures where the paramagnetic metallic state appears in all samples.

Since Mott physics is clearly important in driving anti-ferromagnetic and insulating phases of nickelates [9,22], we have further tested the above DFT results with the inclusion of the self-energy correction due to electron-electron correlations. We compute the complex self-energy effects due to density-density fluctuations within the DFT+MRDF theory [59–62]. The MRDF method directly incorporates the materials-specific DFT band structure and solves the Hubbard model (with intra- and interband Hubbard

interactions) for the electron-electron correlation part. The electron correlations which arise due to spin and charge density fluctuations are computed within the random-phase approximation. The feedback effects of the correlation to the electronic spectrum are captured within the fluctuation-exchange method and quantified by band- (ν), momentum- (\mathbf{k}), and frequency- (ω) dependent complex self-energy $\Sigma_\nu(\mathbf{k}, \omega)$ corrections. We invoke self-consistency in such a way that the spin and charge correlation functions and the electronic Green's function include the self-energy corrections until the convergence in the self-energy value is reached [51].

The interacting Fermi surface is defined by the poles of the interacting Green's function at $\omega = 0$, which is obtained from the self-consistent solution of $\varepsilon_{\mathbf{k}_F}^\nu + \Sigma'_\nu(\mathbf{k}_F, \omega = 0) = 0$, where $\varepsilon_{\mathbf{k}}^\nu$ denotes the ν th DFT band at momentum \mathbf{k} and Σ'_ν represent the real parts of the self-energy. We note that since self-energy is momentum dependent, the above solution can lead to a band-dependent change in shape of the Fermi surface. In what follows the \mathbf{k} -dependent self-energy causes a nonrigid-band shift of the Fermi surface, yet the total Fermi surface volume remains unchanged. This FS volume calculated with the self-energy dressed bands is shown in Fig. 4(c) (middle panel). As seen, we obtain a nonmonotonic behavior of the FS volume across different samples. However, in all cases, we find a one-to-one correspondence with the noninteracting FS volume, in that the electron pocket volume is lower than that of the hole pocket one, except for NNO on YAO. Thus, a strain-induced n -type metallic phase of the NNO film results from the change in relative FS volume by compressive epitaxy.

To further testify that the estimated effective FS volume δv_{FS} truly corresponds to the experimentally observed switching in R_H as a function of ϵ , we plot δv_{FS} as a function of the difference in carrier concentration, $\delta n = n_p - n_e$ (n_p and n_e have been estimated from experimentally determined R_H at 300 K). The linear relation between δv_{FS} and δn shown in Fig. 4(d) clearly testifies to the validity of our approach to capture the experimental observations.

IV. CONCLUSIONS

To summarize, we have synthesized and measured the Hall effect on a series of ultrathin NdNiO₃ films. The selective suppression of the simultaneous transitions in NdNiO₃ films through epitaxial strain engineering enables us to probe the paramagnetic metallic, paramagnetic insulating, and antiferromagnetic insulating phases separately, without any detrimental influence of structural and charge ordering transitions. This approach reveals an unusual sign change in Hall coefficient across the E' -type antiferromagnetic transition. The appearance of such a spin density wave transition from a paramagnetic insulating phase signals that the bond-disproportionation transition creates a partially gapped Fermi surface. Epitaxial strain also drastically changes the relative volume between the hole and electron parts of the Fermi surface, resulting in a strain-driven sign change in R_H in the metallic phase of NNO. Under compressive strain, all of the NNO films exhibit a non-Fermi-liquid behavior with algebraic power exponents, whereas the film under large tensile strain shows magnetotransport behavior akin to the strange-metal phase of optimally doped high- T_c cuprates. While superconductivity remains elusive in the nickelate heterostructures so far, these systems host several remarkable high- T_c cuprate signatures, including the Zhang-Rice state, pseudogap, self-doping, non-Fermi-liquid behavior with linear T resistivity, and spin-density wave.

ACKNOWLEDGMENTS

S.M. acknowledges a IISc start up grant, a DST Nanomission grant (DST/NM/NS/2018/246), and a SERB Early Career Research Award (ECR/2018/001512) for financial support. J.C. is funded by the Gordon and Betty Moore Foundation EPiQS Initiative through Grant No. GBMF4534 and US Department of Energy (DOE) under Grant No. DOE DE-SC 00012375. This research used resources of the Center for Functional Nanomaterials, which is a U.S. DOE Office of Science Facility, at Brookhaven National Laboratory under Contract No. DE-AC02-98CH10886.

-
- [1] M. L. Medarde, *J. Phys.: Condens. Matter* **9**, 1679 (1997).
 - [2] G. Catalan, *Phase Transitions* **81**, 729 (2008).
 - [3] S. Middey, J. Chakhalian, P. Mahadevan, J. W. Freeland, A. J. Millis, and D. D. Sarma, *Annu. Rev. Mater. Res.* **46**, 305 (2016).
 - [4] S. Catalano, M. Gibert, J. Fowlie, J. Íñiguez, J.-M. Triscone, and J. Kreisel, *Rep. Prog. Phys.* **81**, 046501 (2018).
 - [5] T. Mizokawa, D. I. Khomskii, and G. A. Sawatzky, *Phys. Rev. B* **61**, 11263 (2000).
 - [6] U. Staub, G. I. Meijer, F. Fauth, R. Allenspach, J. G. Bednorz, J. Karpinski, S. M. Kazakov, L. Paolasini, and F. d'Acapito, *Phys. Rev. Lett.* **88**, 126402 (2002).
 - [7] S. B. Lee, R. Chen, and L. Balents, *Phys. Rev. Lett.* **106**, 016405 (2011).
 - [8] S. B. Lee, R. Chen, and L. Balents, *Phys. Rev. B* **84**, 165119 (2011).
 - [9] M. K. Stewart, J. Liu, M. Kareev, J. Chakhalian, and D. N. Basov, *Phys. Rev. Lett.* **107**, 176401 (2011).
 - [10] H. Park, A. J. Millis, and C. A. Marianetti, *Phys. Rev. Lett.* **109**, 156402 (2012).
 - [11] S. Johnston, A. Mukherjee, I. Elfimov, M. Berciu, and G. A. Sawatzky, *Phys. Rev. Lett.* **112**, 106404 (2014).
 - [12] M. Hepting, M. Minola, A. Frano, G. Cristiani, G. Logvenov, E. Schierle, M. Wu, M. Bluschke, E. Weschke, H.-U. Habermeier, E. Benckiser, M. Le Tacon, and B. Keimer, *Phys. Rev. Lett.* **113**, 227206 (2014).
 - [13] M. H. Upton, Y. Choi, H. Park, J. Liu, D. Meyers, J. Chakhalian, S. Middey, J.-W. Kim, and P. J. Ryan, *Phys. Rev. Lett.* **115**, 036401 (2015).
 - [14] A. Subedi, O. E. Peil, and A. Georges, *Phys. Rev. B* **91**, 075128 (2015).

- [15] D. Meyers, J. Liu, J. W. Freeland, S. Middey, M. Kareev, J. Kwon, J. M. Zuo, Y.-D. Chuang, J. W. Kim, P. J. Ryan *et al.*, *Sci. Rep.* **6**, 27934 (2016).
- [16] R. J. Green, M. W. Haverkort, and G. A. Sawatzky, *Phys. Rev. B* **94**, 195127 (2016).
- [17] V. Bisogni, S. Catalano, R. J. Green, M. Gibert, R. Scherwitzl, Y. Huang, V. N. Strocov, P. Zubko, S. Balandeh, J.-M. Triscone *et al.*, *Nat. Commun.* **7**, 13017 (2016).
- [18] K. Haule and G. L. Pascut, *Sci. Rep.* **7**, 10375 (2017).
- [19] B. Mandal, S. Sarkar, S. K. Pandey, P. Mahadevan, C. Franchini, A. J. Millis, and D. D. Sarma, [arXiv:1701.06819](https://arxiv.org/abs/1701.06819).
- [20] Y. Lu, D. Betto, K. Fürsich, H. Suzuki, H.-H. Kim, G. Cristiani, G. Logvenov, N. B. Brookes, E. Benckiser, M. W. Haverkort, G. Khaliullin, M. Le Tacon, M. Minola, and B. Keimer, *Phys. Rev. X* **8**, 031014 (2018).
- [21] S. Middey, D. Meyers, M. Kareev, Y. Cao, X. Liu, P. Shafer, J. W. Freeland, J.-W. Kim, P. J. Ryan, and J. Chakhalian, *Phys. Rev. Lett.* **120**, 156801 (2018).
- [22] A. Mercy, J. Bieder, J. Íñiguez, and P. Ghosez, *Nat. Commun.* **8**, 1677 (2017).
- [23] J. Shamblin, M. Heres, H. Zhou, J. Sangoro, M. Lang, J. Neuefeind, J. A. Alonso, and S. Johnston, *Nat. Commun.* **9**, 86 (2018).
- [24] J. Chaloupka and G. Khaliullin, *Phys. Rev. Lett.* **100**, 016404 (2008).
- [25] P. Hansmann, X. Yang, A. Toschi, G. Khaliullin, O. K. Andersen, and K. Held, *Phys. Rev. Lett.* **103**, 016401 (2009).
- [26] P. Hansmann, A. Toschi, X. Yang, O. K. Andersen, and K. Held, *Phys. Rev. B* **82**, 235123 (2010).
- [27] M. J. Han, X. Wang, C. A. Marianetti, and A. J. Millis, *Phys. Rev. Lett.* **107**, 206804 (2011); **110**, 179904(E) (2013).
- [28] E. Benckiser, M. W. Haverkort, S. Brück, E. Goering, S. Macke, A. Frañó, X. Yang, O. K. Andersen, G. Cristiani, H.-U. Habermeier, A. V. Boris, I. Zegkinoglou, P. Wochner, H.-J. Kim, V. Hinkov, and B. Keimer, *Nat. Mater.* **10**, 189 (2011).
- [29] J. W. Freeland, J. Liu, M. Kareev, B. Gray, J. W. Kim, P. J. Ryan, R. Pentcheva, and J. Chakhalian, *Europhys. Lett.* **96**, 57004 (2011).
- [30] J. Chakhalian, J. M. Rondinelli, J. Liu, B. A. Gray, M. Kareev, E. J. Moon, N. Prasai, J. L. Cohn, M. Varela, I. C. Tung, M. J. Bedzyk, S. G. Altendorf, F. Strigari, B. Dabrowski, L. H. Tjeng, P. J. Ryan, and J. W. Freeland, *Phys. Rev. Lett.* **107**, 116805 (2011).
- [31] M. Wu, E. Benckiser, M. W. Haverkort, A. Frano, Y. Lu, U. Nwankwo, S. Brück, P. Audehm, E. Goering, S. Macke, V. Hinkov, P. Wochner, G. Christiani, S. Heinze, G. Logvenov, H.-U. Habermeier, and B. Keimer, *Phys. Rev. B* **88**, 125124 (2013).
- [32] A. S. Disa, F. J. Walker, S. Ismail-Beigi, and C. H. Ahn, *APL Mater.* **3**, 062303 (2015).
- [33] S. Middey, D. Meyers, D. Doennig, M. Kareev, X. Liu, Y. Cao, Z. Yang, J. Shi, L. Gu, P. J. Ryan, R. Pentcheva, J. W. Freeland, and J. Chakhalian, *Phys. Rev. Lett.* **116**, 056801 (2016).
- [34] N. P. Ong and P. W. Anderson, *Phys. Rev. Lett.* **78**, 977 (1997).
- [35] Y. Ando, Y. Kurita, S. Komiya, S. Ono, and K. Segawa, *Phys. Rev. Lett.* **92**, 197001 (2004).
- [36] S. Ono, S. Komiya, and Y. Ando, *Phys. Rev. B* **75**, 024515 (2007).
- [37] N. Nagaosa and Y. Tokura, *Nat. Nanotechnol.* **8**, 899 (2013).
- [38] S.-W. Cheong, H. Hwang, B. Batlogg, A. Cooper, and P. Canfield, *Phys. B (Amsterdam, Neth.)* **194–196**, 1087 (1994).
- [39] D. LeBoeuf, N. Doiron-Leyraud, J. Levallois, R. Daou, J.-B. Bonnemaison, N. Hussey, L. Balicas, B. Ramshaw, R. Liang, D. Bonn *et al.*, *Nature (London)* **450**, 533 (2007).
- [40] H.-T. Kim, Y. W. Lee, B.-J. Kim, B.-G. Chae, S. J. Yun, K.-Y. Kang, K.-J. Han, K.-J. Yee, and Y.-S. Lim, *Phys. Rev. Lett.* **97**, 266401 (2006).
- [41] L. M. Galvin, R. S. Perry, A. W. Tyler, A. P. Mackenzie, S. Nakatsui, and Y. Maeno, *Phys. Rev. B* **63**, 161102(R) (2001).
- [42] H. Xing, L. Wen, C. Shen, J. He, X. Cai, J. Peng, S. Wang, M. Tian, Z.-A. Xu, W. Ku, Z. Mao, and Y. Liu, *Phys. Rev. B* **97**, 041113(R) (2018).
- [43] J. E. Lorenzo, J. L. Hodeau, L. Paolasini, S. Lefloch, J. A. Alonso, and G. Demazeau, *Phys. Rev. B* **71**, 045128 (2005).
- [44] V. Scagnoli, U. Staub, M. Janousch, A. M. Mulders, M. Shi, G. I. Meijer, S. Rosenkranz, S. B. Wilkins, L. Paolasini, J. Karpinski, S. M. Kazakov, and S. W. Lovesey, *Phys. Rev. B* **72**, 155111 (2005).
- [45] V. Scagnoli, U. Staub, A. M. Mulders, M. Janousch, G. I. Meijer, G. Hammerl, J. M. Tonnerre, and N. Stojic, *Phys. Rev. B* **73**, 100409(R) (2006).
- [46] J. Liu, M. Kargarian, M. Kareev, B. Gray, P. J. Ryan, A. Cruz, N. Tahir, Y.-D. Chuang, J. Guo, J. M. Rondinelli, J. W. Freeland, G. A. Fiete, and J. Chakhalian, *Nat. Commun.* **4**, 2714 (2013).
- [47] E. Mikheev, A. J. Hauser, B. Himmetoglu, N. E. Moreno, A. Janotti, C. G. Van de Walle, and S. Stemmer, *Sci. Adv.* **1**, e1500797 (2015).
- [48] A. J. Hauser, E. Mikheev, N. E. Moreno, J. Hwang, J. Y. Zhang, and S. Stemmer, *Appl. Phys. Lett.* **106**, 092104 (2015).
- [49] S. Middey, D. Meyers, S. K. Ojha, M. Kareev, X. Liu, Y. Cao, J. W. Freeland, and J. Chakhalian, *Phys. Rev. B* **98**, 045115 (2018).
- [50] S.-S. Lee, *Annu. Rev. Condens. Matter Phys.* **9**, 227 (2018).
- [51] See Supplemental Material at <http://link.aps.org/supplemental/10.1103/PhysRevB.99.235153> for [RHEED, x-ray diffraction, Hall resistance, resistivity analysis, evaluation of carrier concentration, details of the MRDF method and calculation of spin susceptibility].
- [52] E. C. Jones, D. K. Christen, J. R. Thompson, R. Feenstra, S. Zhu, D. H. Lowndes, J. M. Phillips, M. P. Siegal, and J. D. Budai, *Phys. Rev. B* **47**, 8986 (1993).
- [53] A. J. Hauser, E. Mikheev, N. E. Moreno, T. A. Cain, J. Hwang, J. Y. Zhang, and S. Stemmer, *Appl. Phys. Lett.* **103**, 182105 (2013).
- [54] G. Kresse and J. Furthmüller, *Comput. Mater. Sci.* **6**, 15 (1996).
- [55] G. Kresse and J. Furthmüller, *Phys. Rev. B* **54**, 11169 (1996).
- [56] J. P. Perdew, K. Burke, and M. Ernzerhof, *Phys. Rev. Lett.* **77**, 3865 (1996).
- [57] P. E. Blöchl, *Phys. Rev. B* **50**, 17953 (1994).
- [58] G. Kresse and D. Joubert, *Phys. Rev. B* **59**, 1758 (1999).
- [59] R. S. Dhaka, T. Das, N. C. Plumb, Z. Ristic, W. Kong, C. E. Matt, N. Xu, K. Dolui, E. Razzoli, M. Medarde, L. Patthey, M. Shi, M. Radović, and J. Mesot, *Phys. Rev. B* **92**, 035127 (2015).
- [60] T. Das, J.-X. Zhu, and M. J. Graf, *Phys. Rev. Lett.* **108**, 017001 (2012).
- [61] T. Das and K. Dolui, *Phys. Rev. B* **91**, 094510 (2015).
- [62] T. Das, R. Markiewicz, and A. Bansil, *Adv. Phys.* **63**, 151 (2014).

- [63] J.-S. Zhou, J. B. Goodenough, and B. Dabrowski, *Phys. Rev. Lett.* **94**, 226602 (2005).
- [64] J. Ruppen, J. Teyssier, O. E. Peil, S. Catalano, M. Gibert, J. Mravlje, J.-M. Triscone, A. Georges, and D. van der Marel, *Phys. Rev. B* **92**, 155145 (2015).
- [65] E. F. Schwier, R. Scherwitzl, Z. Vydrova, M. Garcıa-Fernandez, M. Gibert, P. Zubko, M. G. Garnier, J.-M. Triscone, and P. Aebi, *Phys. Rev. B* **86**, 195147 (2012).
- [66] A. Damascelli, Z. Hussain, and Z.-X. Shen, *Rev. Mod. Phys.* **75**, 473 (2003).
- [67] J. S. Lee, S. J. Moon, B. J. Yang, J. Yu, U. Schade, Y. Yoshida, S.-I. Ikeda, and T. W. Noh, *Phys. Rev. Lett.* **98**, 097403 (2007).
- [68] T. Shimojima, T. Sonobe, W. Malaeb, K. Shinada, A. Chainani, S. Shin, T. Yoshida, S. Ideta, A. Fujimori, H. Kumigashira, K. Ono, Y. Nakashima, H. Anzai, M. Arita, A. Ino, H. Namatame, M. Taniguchi, M. Nakajima, S. Uchida, Y. Tomioka, T. Ito, K. Kihou, C. H. Lee, A. Iyo, H. Eisaki, K. Ohgushi, S. Kasahara, T. Terashima, H. Ikeda, T. Shibauchi, Y. Matsuda, and K. Ishizaka, *Phys. Rev. B* **89**, 045101 (2014).
- [69] S. J. Allen, A. J. Hauser, E. Mikheev, J. Y. Zhang, N. E. Moreno, J. Son, D. G. Ouellette, J. Kally, A. Kozhanov, L. Balents, and S. Stemmer, *APL Mater.* **3**, 062503 (2015).
- [70] S. D. Ha, R. Jaramillo, D. M. Silevitch, F. Schoofs, K. Kerman, J. D. Baniecki, and S. Ramanathan, *Phys. Rev. B* **87**, 125150 (2013).
- [71] J. Son, P. Moetakef, J. M. LeBeau, D. Ouellette, L. Balents, S. J. Allen, and S. Stemmer, *Appl. Phys. Lett.* **96**, 062114 (2010).
- [72] R. Eguchi, A. Chainani, M. Taguchi, M. Matsunami, Y. Ishida, K. Horiba, Y. Senba, H. Ohashi, and S. Shin, *Phys. Rev. B* **79**, 115122 (2009).
- [73] H. K. Yoo, S. I. Hyun, L. Moreschini, H.-D. Kim, Y. J. Chang, C. H. Sohn, D. W. Jeong, S. Sinn, Y. S. Kim, A. Bostwick, E. Rotenberg, J. H. Shim, and T. W. Noh, *Sci. Rep.* **5**, 8746 (2015).
- [74] J. Ruppen, J. Teyssier, I. Ardizzone, O. E. Peil, S. Catalano, M. Gibert, J.-M. Triscone, A. Georges, and D. van der Marel, *Phys. Rev. B* **96**, 045120 (2017).
- [75] P. Gegenwart, Q. Si, and F. Steglich, *Nat. Phys.* **4**, 186 (2008).
- [76] N. Doiron-Leyraud, P. Auban-Senzier, S. Rene de Cotret, C. Bourbonnais, D. Jerome, K. Bechgaard, and L. Taillefer, *Phys. Rev. B* **80**, 214531 (2009).
- [77] L. Taillefer, *Annu. Rev. Condens. Matter Phys.* **1**, 51 (2010).
- [78] G. R. Stewart, *Rev. Mod. Phys.* **83**, 1589 (2011).
- [79] B. Keimer, S. A. Kivelson, M. R. Norman, S. Uchida, and J. Zaanen, *Nature (London)* **518**, 179 (2015).
- [80] S. Banerjee, C. Dasgupta, S. Mukerjee, T. Ramakrishnan, and K. Sarkar, *AIP Conf. Proc.* **2005**, 020001 (2018).
- [81] T. R. Chien, Z. Z. Wang, and N. P. Ong, *Phys. Rev. Lett.* **67**, 2088 (1991).
- [82] K. Rajeev, G. Shivashankar, and A. Raychaudhuri, *Solid State Commun.* **79**, 591 (1991).
- [83] P. W. Anderson, *Phys. Rev. Lett.* **67**, 2092 (1991).
- [84] J. M. Harris, H. Wu, N. P. Ong, R. L. Meng, and C. W. Chu, *Phys. Rev. B* **50**, 3246 (1994).
- [85] Y. Li, W. Tabis, G. Yu, N. Barišic, and M. Greven, *Phys. Rev. Lett.* **117**, 197001 (2016).
- [86] S. Stemmer and S. J. Allen, *Rep. Prog. Phys.* **81**, 062502 (2018).
- [87] M. Uchida, Y. Yamasaki, Y. Kaneko, K. Ishizaka, J. Okamoto, H. Nakao, Y. Murakami, and Y. Tokura, *Phys. Rev. B* **86**, 165126 (2012).
- [88] Y. Onose, Y. Taguchi, K. Ishizaka, and Y. Tokura, *Phys. Rev. Lett.* **87**, 217001 (2001).
- [89] S. Badoux, W. Tabis, F. Laliberte, G. Grissonnanche, B. Vignolle, D. Vignolles, J. Beard, D. Bonn, W. Hardy, R. Liang *et al.*, *Nature (London)* **531**, 210 (2016).
- [90] R. Boyack, X. Wang, Q. Chen, and K. Levin, *Phys. Rev. B* **99**, 134504 (2019).
- [91] Y. Dagan and R. L. Greene, *Phys. Rev. B* **76**, 024506 (2007).
- [92] Y. Dagan, M. M. Qazilbash, C. P. Hill, V. N. Kulkarni, and R. L. Greene, *Phys. Rev. Lett.* **92**, 167001 (2004).
- [93] T. Das, R. Markiewicz, and A. Bansil, *J. Phys. Chem. Solids* **69**, 2963 (2008).